Water-Catalyzed Hydrolysis of the Radical Cation of Ketene in the Gas Phase: Theory and Experiment[†]

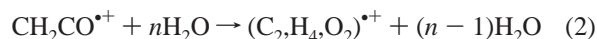## Galina Orlova,*,[‡] Voislav Blagojevic, and Diethard K. Bohme*

Department of Chemistry, Centre for Research in Mass Spectrometry and Centre for Research in Earth and Space Science, York University, 4700 Keele Street, Toronto, Ontario, Canada M3J 1P3

Received: September 21, 2005; In Final Form: November 4, 2005

Both theoretical and experimental investigations are reported for the gas-phase hydrolysis of the radical cation of ketene, $H_2CCO^{\bullet+}$. Density functional theory (DFT) with the B3LYP/6-311++G(d,p) method indicates that a second water molecule is required as a catalyst for the addition of water across the $C=O$ bond in $H_2CCO^{\bullet+}$ by eliminating the activation barrier for the conversion of $[H_2CCO \cdot H_2O]^{\bullet+}$ to $[H_2CC(OH)_2]^{\bullet+}$. Theory further indicates that $[H_2CC(OH)_2 \cdot H_2O]^{\bullet+}$ may recombine with electrons to produce neutral acetic acid. Experimental results of flow-reactor tandem mass spectrometer experiments in which $CH_2CO^{\bullet+}$ ions were produced either directly from ketene by electron transfer or by the chemical reaction of $CH_2^{\bullet+}$ with CO are consistent with formation of an $(C_2,H_4,O_2)^{\bullet+}$ ion in a reaction second-order in H_2O. Furthermore, comparative multi-CID experiments indicate that this ion is likely to be the enolic $CH_2C(OH)_2^{\bullet+}$ cation. The results suggest a possible mechanism for the formation of acetic acid from ketene and water on icy surfaces in hot cores and interstellar clouds.

1. Introduction

Organic synthesis can be initiated in the gas phase by ionizing radiation and achieved through the occurrence of ion−molecule reactions. This is the case, for example, in the interstellar medium where ions are produced by cosmic and ultraviolet radiation. Synthetic reaction schemes involving ions recently have been proposed for the formation in these environments of large organic and biological molecules including amino acids and peptides.[1−3] A suggested gas-phase interstellar synthesis of glycine and β-alanine, for example, requires the prior formation of carboxylic acids.[3] Acetic acid has been detected in the interstellar environment[4] where acetic acid cations may be formed and neutralized.[3] Ionized acetic acid has been proposed to be formed from intermediate ketene cations according to reactions 1 and 2 in which a water molecule can

$$CH_2^{\bullet+} + CO \rightarrow CH_2CO^{\bullet+} \qquad (1)$$

$$CH_2CO^{\bullet+} + nH_2O \rightarrow (C_2,H_4,O_2)^{\bullet+} + (n-1)H_2O \quad (2)$$

act as a catalyst.[3] Reaction 1 constructs the ketene cation from the addition of CO to the methylene cation (by radiative or collisional association) and the ketene cation then is hydrolyzed according to reaction 2. Reaction 2 is the analogue of the hydrolysis of neutral CH_2CO that has been examined theoretically by Nguyen and Raspoet.[5] With neutral CH_2CO, the limiting kinetic barriers to the hydrolysis of the $C=O$ and $C=C$ bonds with a single water molecule were found to be 41.1 and 41.4 kcal mol^{-1}, respectively. The catalytic action of two additional water molecules drops these barriers to 19 and 20

SCHEME 1
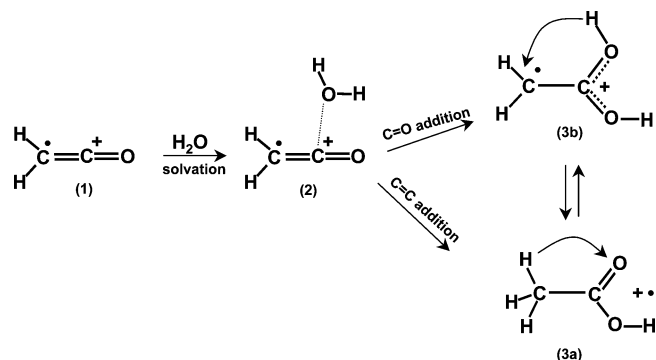
kcal mol^{-1}, respectively, whereas further water molecules appear to be ineffective.[5]

Here we apply theory and experiment to the occurrence and mechanism of the ionic reactions (2) that are proposed to yield tautomers of ionized acetic acid. We shall consider in turn (1) the solvation of $CH_2CO^{\bullet+}$ with a single water molecules as an initial step of hydrolysis, (2) the mechanisms of hydration of the $C=C$ and $C=O$ bonds of $CH_2CO^{\bullet+}$ with a single molecule of water (Scheme 1), and (3) the role of a second water molecule as a catalyst in the formation of ionized acetic acid.

A flow reactor/ tandem mass spectrometer[6] was employed to elucidate the kinetics of the hydrolysis reaction 2 and the structure of the product cation. The latter is attempted with comparative multicollision induced dissociation experiments in which the breakdown of the product ion of reaction 2 is compared with that of ionized acetic acid.

2. Theoretical Methods

All theoretical predictions were made with the GAUSSIAN98 package.[7] Density functional theory was employed to determine optimized geometries, energetics, and natural atomic charges.

Hydrolysis of the Radical Cation of Ketene

J. Phys. Chem. A, Vol. 110, No. 27, 2006 **8267**

The B3LYP functional with Becke's three-parameter hybrid exchange (B3)[8] and correlation functional of Lee, Yang and Parr (LYP)[9] was used.

The triple-zeta 6-311++G(d, p) basis set[10,11] with diffuse and polarization functions on the heavy and hydrogen atoms[12,13] was used predominantly. Harmonic vibrational frequencies were computed to verify minima (all real frequencies) and transition state structures (one imaginary frequency). The connections between transition states and adjacent minima were verified using the intrinsic reaction coordinate technique (IRC) developed by Gonzalez and Schlegel.[14,15] Natural population atomic (NPA) charges were determined using the natural bond orbital (NBO) analysis of Reed and Weinhold.[16−19] To analyze the charge and spin distribution, molecular orbital (Kohn−Sham orbital) plots were constructed using the GaussViewW software package.[20] All energies include zero-point vibrational energy corrections.

3. Experimental Methods

The flow reactor/tandem mass spectrometer used in these experiments is a selected ion flow tube (SIFT) tandem mass spectrometer that consists of two quadrupole mass filters separated by a stainless steel flow tube.[6] Helium flows through the tube at a constant pressure of 0.35 Torr and room temperature (294 ± 3 K). Ions are generated in an ion source separated from the flow tube by a quadrupole mass filter. Then they enter the flow tube upstream through a Venturi-type aspirator. The ions react downstream with added reactant molecules and then are sampled through a nose cone and analyzed with a second quadrupole mass filter. The ions derived from the ion source or generated upstream by chemical reaction before they enter the reaction region downstream are thermalized by collisions with the He buffer-gas atoms. Ketene cations were produced in one of two ways, either by electron transfer from ketene to Ar$^{\bullet+}$ ions created in an Inductively Coupled Plasma (ICP) ion source or by ion/molecule reactions of CH$_2$$^{\bullet+}$ ions with CO within an electron-impact (EI) ion source. The methane (Matheson/BOC, UHP grade, 99.98%) and CO (Air Liquide, CP grade, 99.5%) were of high purity. The ketene was obtained by distilling commercially available diketene (Aldrich, 99.9%). Some diketene ions were observed in our experiments, due to either partial dimerization of the ketene sample during the experiments or incomplete distillation of the commercially obtained diketene. These ions did not participate in the chemistry that leads to the formation of acetic acid cations; only slow clustering with water was observed.

Some fragmentation of ketene cations was observed either by dissociative electron transfer from ketene to Ar$^{\bullet+}$ in the ICP/SIFT experiments or because of incomplete stabilization in the EI/SIFT experiments. However, because the resulting cations were of low mass/charge ratio (CH$_2$$^{\bullet+}$, CO$^{\bullet+}$ eventually producing H$_2$O$^{\bullet+}$ and H$_3$O$^+$ through ion/molecule reactions), they did not interfere with the experiments. In some of our experiment D$_2$O (Aldrich, 99% isotopically pure) was used instead of H$_2$O to distinguish reagent D$_2$O from the background H$_2$O present in the helium buffer gas. Water was added as a 2% mixture of vapor in helium. Bond connectivities within the sampled ions were explored by changing the nose cone potential and thereby inducing multi-collisional dissociation (CID).[21] In these latter experiments higher collision energies were achieved by replacing the helium buffer gas with argon at ∼0.14 Torr. In the comparative CID experiments acetic acid (Aldrich, >99.7%) was used as a source of acetic acid cations.

4. Theoretical Results

a. Hydration of the Radical Cation of Ketene with a Single Water Molecule. As a first step on the synthetic rout to acetic acid, radical-cation ketene undergoes solvolysis and forms complexes with water molecules. The structures, selected geometries, and plots of selected molecular orbitals for the radical cation of ketene and its complexes with a water molecule as predicted with the B3LYP/6-311++G(d,p) method are depicted in Figure 1. Energetics are presented in Table 1. For ketene, **1**, the singly occupied molecular orbital (SOMO) is a nonbonding π-orbital. An unpaired electron resides essentially on the methylene carbon and partly on the oxygen atom (Mulliken spin densities equal 0.8e and 0.2e, respectively). NPA charges in ketene **1** reveal that the positive charge resides essentially on the carbonyl carbon and partly on hydrogen atoms. The oxygen atom carries a small negative charge. The C−O bond (1.124 Å) is shorter than the corresponding double bond in neutral ketene (1.161 Å with the B3LYP/6-311++G(d,p) method). The corresponding resonance structure, H$_2$C$^{\bullet}$−C≡O$^+$, is distonic,[22] with separated spin and charge sites.

Two different types of the ketene−water interaction can be proposed because the electronic structure of ketene **1** is distonic: (1) the covalent interaction between the highest occupied b$_1$ and a$_1$ molecular orbitals of water molecule and SOMO of ketene, **1**, and (2) the ion−dipole interaction between the two moieties. The former corresponds to the "out-of-plane" attack of the water molecule on the ketene **1**, whereas the latter results from the "in-plane" attack as sketched in Scheme 2.

The in-plane attack leads to the complexes **2a** and **2b**, with the water molecule attached to the carbon atom carrying the greater positive charge, +0.79, and to the hydrogen atom carrying a smaller positive charge, +0.29, respectively. For **2a** and **2b**, a natural bond orbital (NBO) analysis shows no interactions between the molecular orbitals of the water molecule and ketene. This is consistent with the negative O···C and O···H Mulliken populations for **2a** and **2b**. For both complexes, a natural population analysis indicates only a minor transfer of electron density from the water molecule to ketene. The positive charge accumulated by the water moiety is +0.05 and +0.06, respectively. Thus, **2a** and **2b** are assigned to ion−dipole complexes. These results are in general accord with the theoretical HF/6-31G**//4-31G examination of the [CH$_2$CO·H$_2$O]$^{\bullet+}$ radical cation in the pioneering work reported by Postma et al.[23] Structures **2a** and **2b** were located in this study and the ion−dipole nature of the bonding was proposed. Because the potential energy surface is nearly flat, these authors also suggested the free motion of water molecule about the ketene at energies below the dissociation limit to CH$_2$CO$^{\bullet+}$ + H$_2$O. In contrast to previous HF/6-31G**//4-31G results, the B3LYP/6-311++G(d,p) method does not yield the complexes with water molecule attached to the carbonyl oxygen or to two hydrogen atoms: the former leads to complex **2a**, whereas the latter leads to the out-of-plane complex **2c** (Figure 1), which has not been previously reported. The **2c** complex also results upon a direct "out-of-plane" attack of the water molecule (Scheme 2) on the π-system of ketene. The **2c** structure has a C_s symmetry, with the water molecule shifted to the methylene carbon atom. The binding molecular orbitals of **2c** in Figure 1 indicate clearly a covalent interaction between the two moieties. According to a NBO analysis, the contributions of the carbon atom of ketene and the oxygen atom of water in the covalent bonding are ca. 10 and 90%, respectively. In accord with NBO, a Mulliken analysis yields a small but notable positive C···O
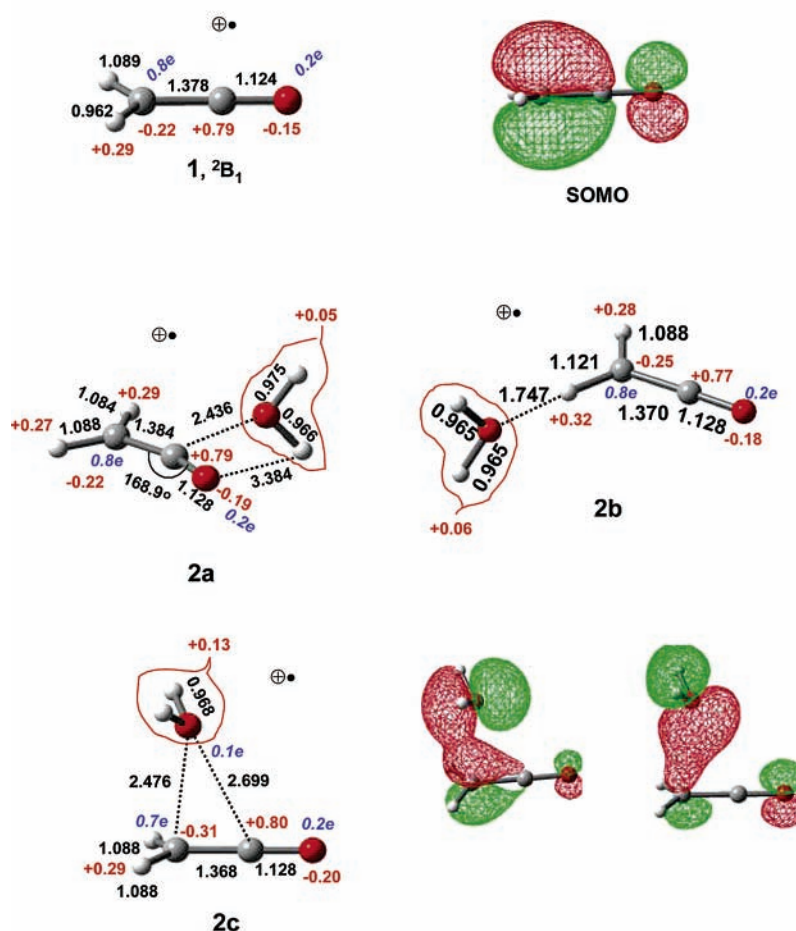
Figure 1. Structures and selected geometries predicted for CH$_2$CO$^{\bullet+}$ and its complexes with a single water molecule using the B3LYP/6-311++G-(d,p) method. Bond lengths are in Å, and angles are in degrees. NPA charges (red) and Mulliken spin densities (blue italics) are reported. The singly occupied molecular orbital (SOMO) is shown for ketene **1**. For **2c**, the two highest doubly occupied binding molecular orbitals are reported.

TABLE 1: Energetics Predicted for the Hydrolysis of H$_2$CCO$^{\bullet+}$ with a Single Water Molecule (Top) and for Neutral Forms of Acetic Acid and the Transition Structure between Them (Bottom) Using the B3LYP/6-311++G(d,p) Method

system	H_0	G_{298}	ΔH_0	ΔG_{298}	IE
H$_2$O	−76.43725	−76.45489			
H$_2$CCO$^{\bullet+}$	−152.26508	−152.28874			
H$_2$CCO$^{\bullet+}$ + H$_2$O	−228.70233	−228.74363	0.0	0.0	
2a	−228.72726	−228.75739	−15.6	−8.6	
2b	−228.72731	−228.75796	−15.7	−9.0	
2c	−228.72770	−228.75783	−15.9	−8.9	
TS(**2a-3a**)	−228.65018	−228.67769	32.7	41.4	
TS(**2a-3b**)	−228.67399	−228.70091	17.8	26.8	
3a, CH$_3$COOH$^{\bullet+}$	−228.71762	−228.74524	−9.6	−1.0	
3b, CH$_2$COHOH$^{\bullet+}$	−228.74746	−228.77438	−28.3	−19.3	
TS(**3a-3b**)	−228.67528	−228.70202	17.0	26.1	
5a, CH$_3$COOH	−229.10330	−229.13054	0.0	0.0	242.0
5b, CH$_2$COHOH	−229.05966	−229.08674	27.4	27.5	195.9
TS (**5b-5a**)	−228.99008	−229.01614	71.0	71.8	

^{a} Enthalpies, H_0, and free energies, G_{298}, are in hartrees, relative enthalpies, ΔH_0, relative free energies, ΔG_{298}, and ionization energies, IE, are in kcal mol^{-1}.

population of 0.05. A natural population analysis indicates significant positive charge (+0.13) accumulated on the H$_2$O moiety.

Despite the different nature of bonding, the **2a**, **2b**, and **2c** structures are nearly degenerate in energy, with binding enthalpies at 0 K of ca. 16 kcal mol^{-1} (Table 1). Complexes **2a** and **2c** appear to be candidates for the C=O and C=C hydrolysis. However, only one of them, **2a**, undergoes hydration, with the

SCHEME 2
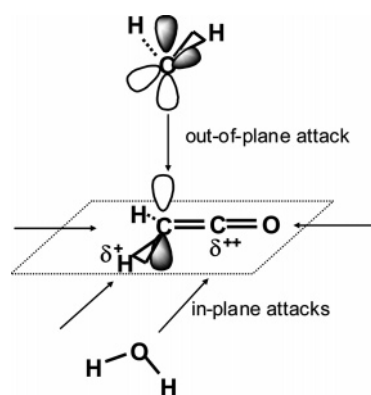
formation of acetic acid. Complex **2c** is reminiscent of "unreactive" solvation, which has been found in theoretical ab initio molecular dynamics (AIMD) studies of ethylene radical cation in water by Mohr et al.[24] The unreactive [H$_2$CCH$_2$·(H2O)$_n$]$^{\bullet+}$ complexes from the AIMD study are apparently π-complexes, similar to **2c**. The "reactive" [H$_2$CCH$_2$·(H2O)$_n$]$^{\bullet+}$ complexes located by Mohr et al.[24] are similar to **2a**, i.e., ion−dipole complexes.

The reaction profiles for the hydration of **2a** are shown in Figure 2, the structures and selected geometries are presented in Figure 3, and energetics are listed in Table 1. Structure **2a** is a pre-reaction complex for the two concerted reaction pathways: the hydration of the C=C bond, which results in the keto form of acetic acid, **3a**, and hydration of the C=O bond,

Hydrolysis of the Radical Cation of Ketene

J. Phys. Chem. A, Vol. 110, No. 27, 2006 **8269**
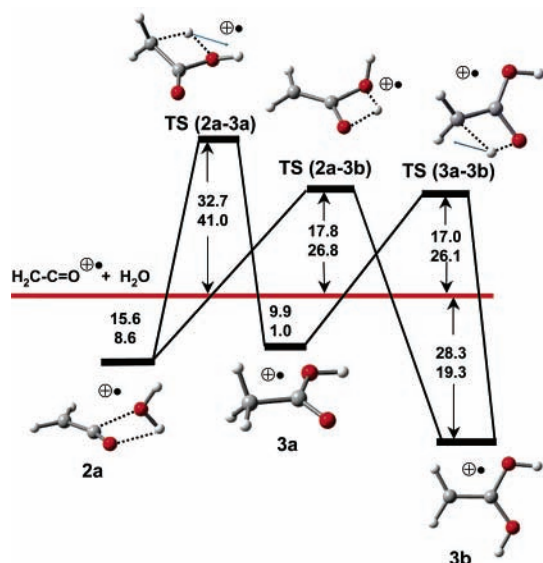
Figure 2. Reaction profiles predicted for the hydrolysis of the C=C and C=O bonds of $CH_2CO^{+\bullet}$ with a single water molecule using the B3LYP/6-311++G(d,p) method. Relative enthalpies at 0 K (top values) and relative free energies at 298 K (bottom values) in kcal mol^{-1} are reported. Transition state vectors are sketched.

TABLE 2: Enthalpies, H_0 (in hartrees), Free Energies, G_{298} (in hartrees), Relative Enthalpies, ΔH_0 (in kcal mol^{-1}), and Relative Free Energies, ΔG_{298} (in kcal mol^{-1}), Predicted for the Hydrolysis of $H_2CCO^{\bullet+}$ with Two Water Molecule with the B3LYP/6-311++G(d,p) Method

| system	H_0	G_{298}	ΔH_0	ΔG_{298}
$H_2CCO^{\bullet+}$ + $2H_2O$	−305.13958	−305.19853	0.0	0.0
2a + H_2O	−305.16451	−305.21228	−15.6	−8.6
4a	−305.19503	−305.22740	−34.8	−18.1
4b	−305.22082	−305.25351	−51.0	−34.5
TS(**4a-4b**)	−305.19269	−305.22392	−33.3	−15.9
3b + H_2O	−305.18471	−305.22927	−28.3	−19.3

TABLE 3: Proton Affinities PA (in kcal mol^{-1}) of the Neutral Base, H_2O, and the Carbon and Oxygen Sites Predicted with the B3LYP/6-311++G(d,p) Method.[a]

system	H_0	PA
$\underline{\mathbf{H_2O}}$	−76.43725	163.0
$\underline{H_3O}^+$	−76.69695	
$CH_2COOH^\bullet$	−228.45084	
$CH_3COOH^{\bullet+}$	−228.71762	
$CH_2COHOH^{\bullet+}$	−228.74746	
$CH_2C\underline{\mathbf{O}}OH^\bullet$		167.4
$\underline{\overline{CH_2C}}OOH^\bullet$		186.1

[a] The site of protonation is in bold and underlined.

with the formation of enolic, $H_2CC(OH)_2^{\bullet+}$, form, **3b**.[25] Both reactions are exoergic; the enolic structure, **3b**, is 18.4 kcal mol^{-1} lower in terms of enthalpy at 0 K than the keto form, **3a**. Plots of the SOMOs and NPA charges in Figure 3 reveal that the keto acetic acid, **3a**, is a σ-radical, with an unpaired electron on the lone pair of the carbonyl oxygen and a positive charge on the carboxyl carbon. In contrast, the enolic form, **3b**, is a π-radical, with a spin and charge distribution similar to that in ketene, **1**. The hydration of the C=C bond proceeds via a reaction barrier of 48.3 kcal mol^{-1}. The corresponding transition structure, **TS(2a→3a)**, features formation of a C=O bond and the 1,3 shift of a hydrogen atom from the water molecule fragment to the CH_2 group. For the hydration of the C=O bond, the reaction barrier is lower, 33.4 kcal mol^{-1}, but still significant. This reaction proceeds via transition structure, **TS(2a→3b)**, with a C−O bond being formed and a 1,3 shift of proton from the water molecule fragment to the carboxyl oxygen. The keto and enolic forms of acetic acid are separated by a significant energy barrier, as is typical of 1,3 shifts. The transition state structure, **TS(3a→3b)**, is 26.9 kcal mol^{-1} higher in energy than the keto form, **3a**.

b. Reaction of $[H_2CCO\cdot(H_2O)]^{\bullet+}$ with a Water Molecule as Catalyst. There are two most probable sites for the water attack on the pre-reaction complex **2a** in accord with the distribution of positive charge: on the carbonyl carbon and on the hydrogen atom of the attached water molecule. The former attack leads to the symmetric complex depicted in Scheme 3.

SCHEME 3
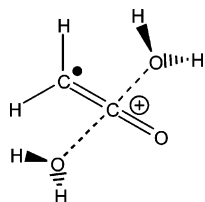
This arrangement does not facilitate the hydrolysis of the C=O bond; the reaction barrier remains essentially the same (structures are not reported). By contrast, the attack on the

hydrogen atom of the attached water leads to an almost barrierless formation of acetic acid. The potential energy profile for this reaction is shown in Figure 4; the structures and selected geometries are depicted in Figure 5. Energies are listed in Table 2. The attack of the water molecule on the hydrogen atom of the attached H_2O in the pre-reaction complex, **2a**, causes the formation of the distonic intermediate, **4a**. In this intermediate, the C−OH distance decreases from 2.436 to 1.565 Å whereas one of the O−H bonds in the attached water molecule is elongated from 0.975 to 1.062 Å. The total natural charge of the $H_2O\cdots H$−OH moiety in **4a** is +0.49; i.e., half of the positive charge is transferred from the ketene radical cation upon the addition of the second water. Such delocalization of the positive charge stabilizes cations in general[25c] and, in the particular case of radical cations, causes further separation of spin and charge sites and so provides specific stabilization for a distonic structure. Thus, the binding enthalpy of the second water is greater than the first one (19.2 and 15.6 kcal mol^{-1}, respectively). The rotation about the putative C−OH bond via very small barrier at 1.5 kcal mol^{-1} places the carbonyl oxygen in a favorable position for the proton attack which proceeds energetically downhill to the $[H_2CC(OH)_2\cdot H_2O]^{\bullet+}$ postreaction complex, **4b**. The reaction enthalpy of −51.0 kcal mol^{-1} provides feasible dissociation of the $[H_2CC(OH)_2\cdot H_2O]^{\bullet+}$ complex to the enolic form of ionized acetic acid, **3b**. A water molecule is released.

c. Possible Mechanisms of the Formation of $CH_3COOH^{\bullet+}$ from $CH_2C(OH)_2^{\bullet+}$. The second water molecule is an efficient catalyst for the hydrolysis of the C=O bond of the radical cation of ketene. The product is the enolic form of the acetic acid cation. Figure 2 shows that the barrier to the 1,3 shift of a proton to achieve the keto form is high and above the dissociation limit. Can a water molecule reduce this barrier by proton-transport catalysis? For exothermic isomerization reactions generally, a previously formulated requirement for proton-transport catalysis says that "the transporter molecule should have a proton affinity not more than about 10 kcal mol^{-1} (depending on the interaction energy of the reactants) lower than the proton affinity of the high-energy site of the protonated molecule, and lower than the proton affinity of the low-energy site of the protonated molecule".[26] The proton affinities of the transporter molecule,
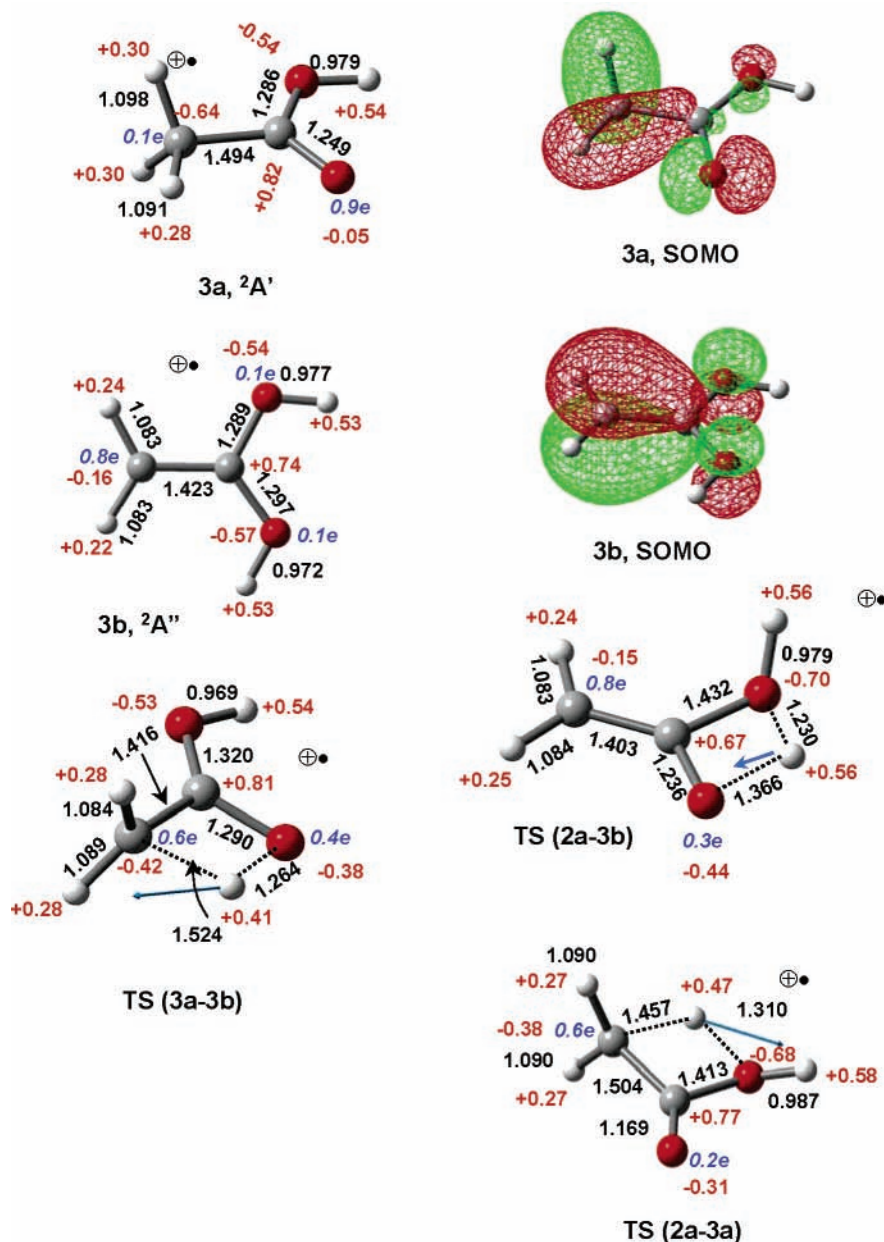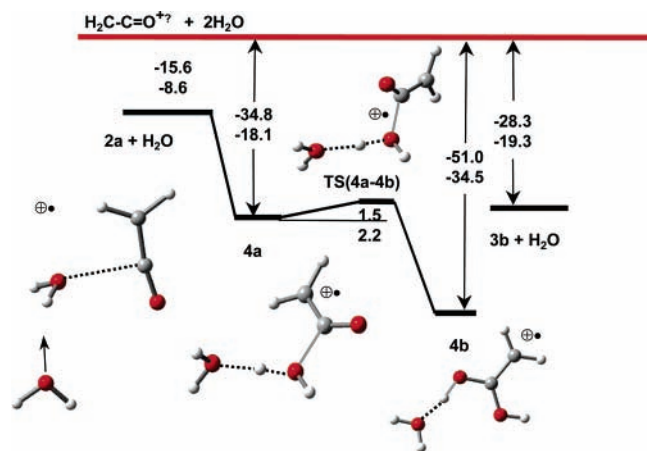
Figure 3. Selected geometries for products and transition state structures predicted for the hydrolysis of $CH_2CO^{\bullet+}$ with a single water molecule using the B3LYP/6-311++G(d,p) method. Bond lengths are in Å. Natural atomic charges (red) and Mulliken spin densities (blue italics) are reported. For selected structures, singly occupied molecular orbitals (SOMO) are shown. Transition state vectors are sketched.

H_2O, and the high-energy (carbon atom) and low-energy (oxygen atom) sites of the radical acetic acid, $CH_2COOH^{\bullet}$, predicted with the B3LYP/6-311++G(d,p) method are 163.0, 167.4, and 186.1 kcal mol^{-1}, respectively (Table 3). Thus PA-(H_2O) is 4.4 kcal mol^{-1} lower than PA of the high-energy site, $\underline{C}H_2COOH^{\bullet}$, and 23.1 kcal mol^{-1} lower than PA of the low-energy site, $CH_2C\underline{O}OH^{\bullet}$. This means that the PAs are suitable for the H_2O molecule to transport a proton from the $CH_3COOH^{\bullet+}$ to the $CH_2C(OH)_2^{\bullet+}$ form. Our interest, however, is in the reverse reaction that is endothermic overall. In this case, the catalysis might be efficient in producing of postreaction complex, $[CH_3COOH \cdot H_2O]^{\bullet+}$.

The reaction profile for the proposed proton transport from $CH_2C(OH)_2^{\bullet+}$ to $CH_3COOH^{\bullet+}$ is shown in Figure 6. Selected geometries of the structures on the reaction pathway are shown in Figure 7; energies are reported in Table 4. For the pre-reaction complex, **4c**, the B3LYP/6-311++G(d,p) method yields the binding enthalpy of 23.6 kcal mol^{-1} and a barrier to proton

transport from **4c** to the postreaction complex $[CH_3COOH \cdot H_2O]^{\bullet+}$, **4d**, of 36.9 kcal mol^{-1} (solid line in Figure 6). Therefore, the water molecule as a carrier of a proton reduces the reaction barrier to 1,3 shift by 8.4 kcal mol^{-1} compared to the noncatalyzed reaction in Figure 2. This catalyzed barrier is still 13.3 kcal mol^{-1} *above* the dissociation limit to $CH_2C(OH)_2^{\bullet+} + H_2O$. Therefore, this reaction cannot be observed experimentally at room temperature. However, the catalyzed barrier is −5.5 kcal mol^{-1} *below* the dissociation limit to $CH_3COOH^{\bullet+} + H_2O$. Thus, the water molecule can effectively transport the aliphatic proton from the keto form, **3a**, to the enolic form, **3b**, at higher temperatures.

The efficacy of proton transport reduces if entropy effects are taken into account. The free energy profile at 298 K reveals that the transition state structure, **TS1(4c-4d)**, is 3.2 kcal mol^{-1} *above* the dissociation limit to $CH_3COOH^{\bullet+} + H_2O$. This can be ascribed to the high density of states of the unbound reactants and the low density of states of the tight **TS1(4c-4d)** for proton

Hydrolysis of the Radical Cation of Ketene

J. Phys. Chem. A, Vol. 110, No. 27, 2006 **8271**

Figure 4. Reaction profile predicted for the catalytic hydrolysis of the C−O bond of the [CH₂CO·H₂O]•⁺ complex with the second water molecule using the B3LYP/6-311++G(d,p) method. Relative enthalpies at 0 K (top values) and relative free energies at 298 K (bottom values) are reported in kcal mol⁻¹.

Figure 6. Potential energy profile for the proton transport reaction CH₂COHOH•⁺ → CH₃COOH•⁺, with water molecule as a carrier, via 1,3-shift mechanism. Relative enthalpies at 0 K (top values) and relative free energies at 298 K (bottom values) are reported in kcal mol⁻¹.
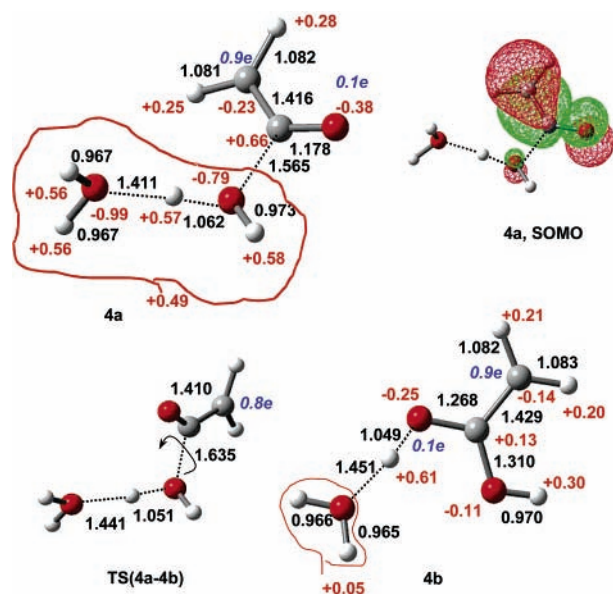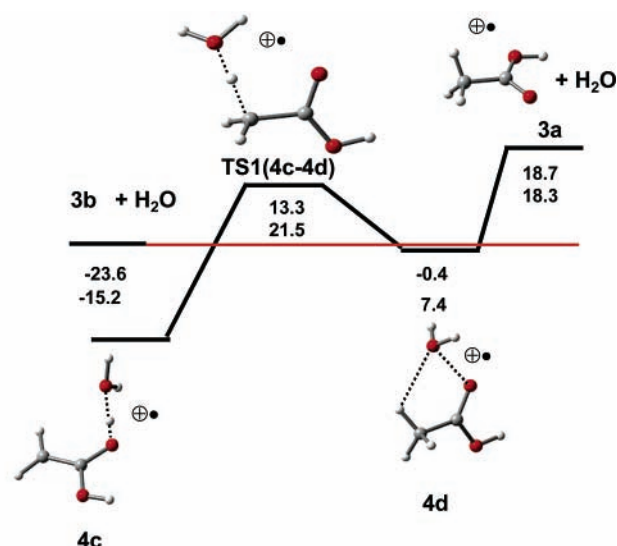

Figure 5. Structures and selected geometries for the intermediates and transition state structure predicted for the catalytic hydrolysis of the C−O bond of the [CH₂CO···H₂O]•⁺ complex with the second water molecule using the B3LYP/6-311++G(d,p) method. Bond lengths are in Å. NPA charges (red) and Mulliken spin densities (blue italics) are reported. The singly occupied molecular orbital (SOMO) is shown.
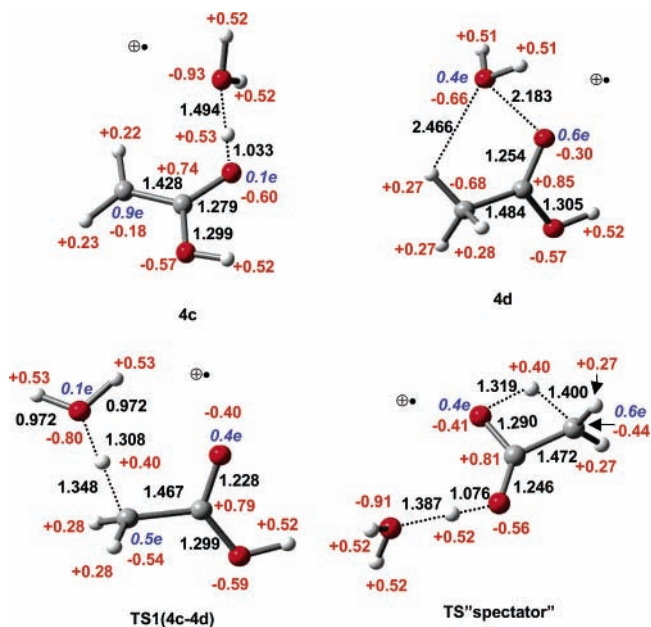

Figure 7. Structures and selected geometries predicted using the B3LYP/6-311++G(d,p) method for proton transport reaction CH₂-COHOH•⁺ → CH₃COOH•⁺, with water molecule as a carrier via 1,3-shift mechanism. Bond lengths are in Å. Natural atomic charges (red) and Mulliken spin densities (blue italics) are reported. The transition state structure for the higher energy mechanism "spectator" is shown.

transport, given the negative entropy $\Delta S^{\ddagger}$ of −28.1 cal mol⁻¹ K⁻¹ (not listed in the tables).

Another possible hydrogen-transfer mechanism involving the transition state structure **TS** "spectator" in Figure 7 also was examined. In this mechanism the water molecule is a mere spectator, coordinated with one of the HO groups. However, the **TS** "spectator" is 6.2 kcal mol⁻¹ higher in terms of enthalpy at 0 K than **TS1(4c→4d)** and, thus, is *above* the dissociation limit to CH₃COOH•⁺ + H₂O.

So the water molecule appears helpless in the transformation of the enolic form, CH₂C(OH)₂•⁺, to the canonic form, CH₃-COOH•⁺, at low temperatures. However, in cold interstellar environments containing free electrons where the enolic form, **4c**, might be produced by the radiative association of H₂O with CH₂C(OH)₂•⁺, **4c** could gain sufficient energy for the re-

arrangement into the canonic form upon electron adsorption according to reaction 3. The reaction barrier to hydrogen transfer

$$[CH_2C(OH)_2 \cdot H_2O]^{\bullet+} + e \rightarrow CH_3COOH + H_2O \quad (3)$$
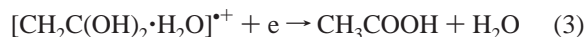
for the neutral enolic form of acetic acid is 43.6 kcal mol⁻¹ (see Figure 8). The IE of neutral enolic form is 195.9 kcal mol⁻¹ (Table 1). Thus, electron attachment to the hydrated radical-cation enolic form, **4c**, may result in the formation of neutral canonic acetic acid.

5. Experimental Results

Kinetics of Hydration of the Radical Cation of Ketene. The computations predict a number of interesting features for
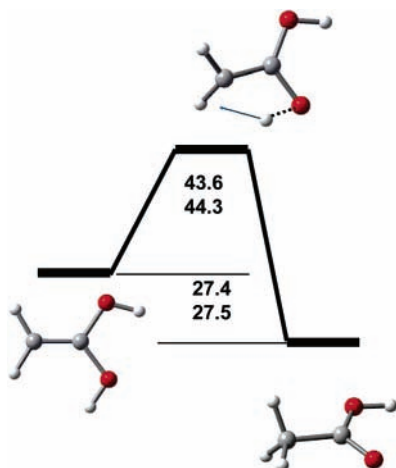
Figure 8. Reaction profile for the 1,3-shift for the unimolecular neutral reaction $CH_2COHOH \rightarrow CH_3COOH$. Relative enthalpies at 0 K (top values) and relative free energies at 298 K (bottom values) in kcal mol^{-1} are reported.

TABLE 4: Enthalpies, H_0 (in hartrees), Free Energies, G_{298} (in hartrees), Relative Enthalpies, ΔH_0 (in kcal mol^{-1}), and Relative Free Energies, ΔG_{298} (in kcal mol^{-1}), Predicted for the Proton Transport Pathways with the B3LYP/6-311++G(d,p) Method.

system	H_0	G_{298}	ΔH_0	ΔG_{298}
3b + H_2O			0.0	0.0
4c	−305.22234	−305.25354	−23.6	−15.2
4d	−305.18537	−305.21736	−0.4	7.4
TS1(**4c-4d**)	−305.16349	−305.19499	13.3	21.5
3a + H_2O	−305.15486	−305.20013	18.7	18.3
TS$_{spectator}$	−305.15362	−305.18601	19.5	27.1

the hydration of the radical cation of ketene. The formation of the electrostatically bonded water adduct **2** for which three nearly isoenergetic structures have been identified (**2a**, **2b**, or **2c**; see Table 1), reaction 4, is predicted to be exoergic by no more than 9 kcal mol^{-1}.

$$\text{ketene}^{\bullet+} + H_2O \rightarrow \text{ketene}^{\bullet+} \cdot H_2O \qquad \Delta G = -9 \quad (4)$$
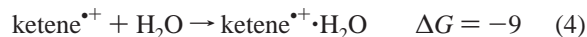
The predicted energy barriers for the hydrolysis of the C−C and C=O bonds of ionized ketene, **1**, to form either tautomer **3a** or **3b** of ionized acetic acid, reactions 5 and 6, respectively,

$$\text{ketene}^{\bullet+} + H_2O \rightarrow \text{enol}^{\bullet+} \qquad \Delta G = -19.3, +26.8 \quad (5)$$

$$\text{ketene}^{\bullet+} + H_2O \rightarrow \text{keto}^{\bullet+} \qquad \Delta G = -1.0, +41.0 \quad (6)$$

are far above the dissociation limit to $H_2C-C-O^{\bullet+}$ and H_2O (see Figure 2). The computed exoergicity and free energy of activation are given along with the reaction equation. Thus, these first-order hydration reactions (both exoergic) should not be experimentally observable at room temperature.

Most interesting is the computed potential energy profile shown in Figure 4 that predicts a second-order exoergic hydration of structure **2a** to form the hydrated enol isomer of ionized acetic acid **3b** that can occur without the intervention of a kinetic barrier because of the catalytic action of the second water molecule, reaction 7.
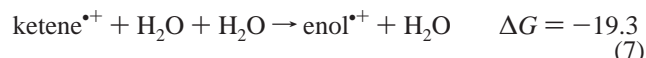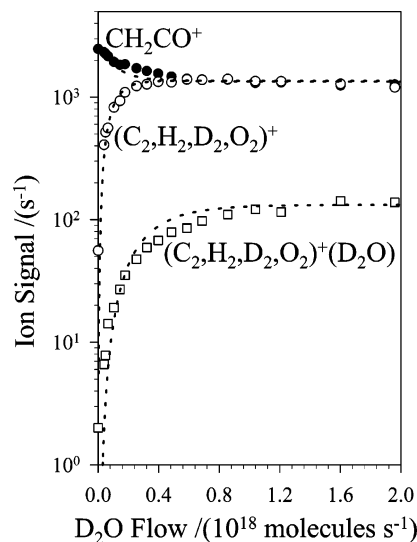
$$\text{ketene}^{\bullet+} + H_2O + H_2O \rightarrow \text{enol}^{\bullet+} + H_2O \qquad \Delta G = -19.3 \quad (7)$$

Figure 9 shows the ion profiles measured with the addition of D_2O into the reaction region of the flow tube in which CH$_2$-

Figure 9. Reaction profile for the reaction of ionized ketene with water. The symbols represent experimental data, and the lines represent the fit modeled after the proposed mechanism (see text). D_2O was used in this case rather than H_2O to differentiate from background water originating from the helium buffer gas. $CH_2CO^{\bullet+}$ was created by reaction electron transfer from neutral ketene to $Ar^{\bullet+}$ created in the ICP ion source. The fitted curves were derived from the mechanism described in the text.

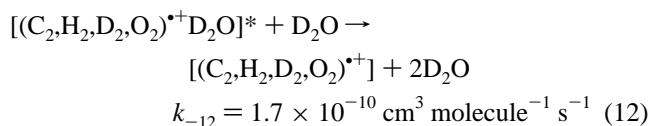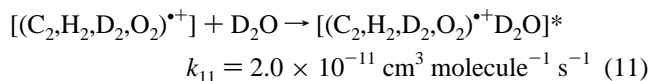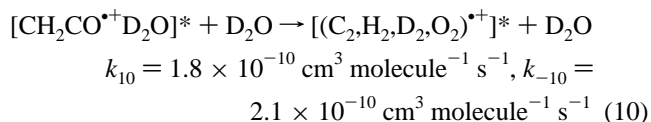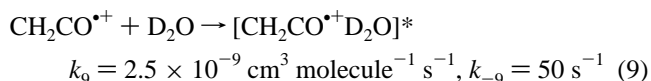$CO^{\bullet+}$ was produced upstream by electron transfer from ketene to $Ar^{\bullet+}$. The decay of $CH_2CO^{\bullet+}$ is seen to be severely curved and both primary ions with composition $(C_2,H_2,D_2,O_2)^{\bullet+}$ and hydrated secondary ions of the type $(C_2,H_2,D_2,O_2)^{\bullet+}H_2O$ were observed to be produced. The primary product formation is qualitatively consistent with the occurrence of reaction 8 with $n = 1$ or 2 in both directions. The initial slope of the decay of
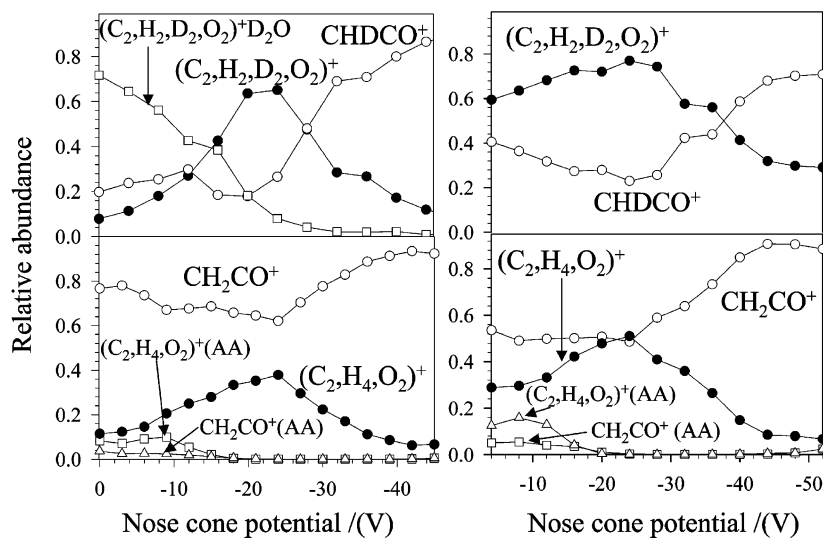
$$CH_2CO^{\bullet+} + nD_2O \rightarrow (C_2,H_2,D_2,O_2)^{\bullet+} + (n-1)D_2O \quad (8)$$
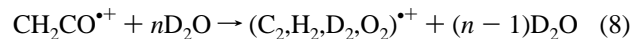
$CH_2CO^{\bullet+}$ ion provides a lower limit to the effective second-order rate coefficient ($n = 1$) of $\geq 2.7 \times 10^{-10}$ cm^3 molecule^{-1} s^{-1} ($\pm 30\%$).

A ratio-plot analysis indicates that reaction 7 does not establish equilibrium under SIFT operating conditions, with $\Delta G°_{295} < -10.2$ kcal mol^{-1}.

Figure 9 includes a fit to the data derived with the following reaction mechanism. The basic features of this mechanism include reversible formation of the D_2O adduct, reaction 9, the reversible enolization of the adduct in the presence of another D_2O molecule, reaction 10, and the reversible hydration of the enol cation, reactions 11 and 12.

$$CH_2CO^{\bullet+} + D_2O \rightarrow [CH_2CO^{\bullet+}D_2O]^*$$
$$k_9 = 2.5 \times 10^{-9} \text{ cm}^3 \text{ molecule}^{-1} \text{ s}^{-1}, k_{-9} = 50 \text{ s}^{-1} \quad (9)$$

$$[CH_2CO^{\bullet+}D_2O]^* + D_2O \rightarrow [(C_2,H_2,D_2,O_2)^{\bullet+}]^* + D_2O$$
$$k_{10} = 1.8 \times 10^{-10} \text{ cm}^3 \text{ molecule}^{-1} \text{ s}^{-1}, k_{-10} =$$
$$2.1 \times 10^{-10} \text{ cm}^3 \text{ molecule}^{-1} \text{ s}^{-1} \quad (10)$$

$$[(C_2,H_2,D_2,O_2)^{\bullet+}] + D_2O \rightarrow [(C_2,H_2,D_2,O_2)^{\bullet+}D_2O]^*$$
$$k_{11} = 2.0 \times 10^{-11} \text{ cm}^3 \text{ molecule}^{-1} \text{ s}^{-1} \quad (11)$$

$$[(C_2,H_2,D_2,O_2)^{\bullet+}D_2O]^* + D_2O \rightarrow$$
$$[(C_2,H_2,D_2,O_2)^{\bullet+}] + 2D_2O$$
$$k_{-12} = 1.7 \times 10^{-10} \text{ cm}^3 \text{ molecule}^{-1} \text{ s}^{-1} \quad (12)$$

Figure 10. Comparison of CID profiles of the product of the reaction of ketene cation with water (top) and ionized acetic acid (bottom). Experiments on the left were performed using the EI ion source. Ketene cations were generated by ion/molecule reactions of $CH_2^{\bullet+}$ with CO, whereas acetic acid was ionized by electron transfer to $CO^{\bullet+}$. Experiments on the right were performed using $Ar^{\bullet+}$ ions from the ICP ion source to generate ketene or acetic acid cations. In the ionic clusters neutral acetic acid is represented as (AA). In all cases argon buffer gas ($P \sim 0.14$ Torr) was used.

Results of the CID measurements performed to try to elucidate the structure of the product ions are shown in Figure 10. Ar was used as the collision gas. The CID profiles of the $(C_2,H_2,D_2,O_2)^{\bullet+}$ product ions of reaction 1 were measured and compared with the CID profiles of $(C_2,H_4,O_2)^{\bullet+}$ ions produced directly from acetic acid vapor by electron transfer to $CO^{\bullet+}$ or $Ar^{\bullet+}$. Specifically, $(C_2,H_2,D_2,O_2)^{\bullet+}$ ions produced from D_2O reacting with $CH_2CO^{\bullet+}$ made in the EI source from $CH_2^{\bullet+}$ + CO were compared with $(C_2,H_4,O_2)^{\bullet+}$ ions derived from acetic acid upstream of the flow tube by electron transfer to $CO^{\bullet+}$ generated in the ion source. The adduct ion $(C_2,H_2,D_2,O_2)^{\bullet+}D_2O$ was predominant at the flow of D_2O employed in this experiment. Also, $(C_2,H_2,D_2,O_2)^{\bullet+}$ ions produced from D_2O reacting with $CH_2CO^{\bullet+}$ made by electron transfer from ketene to $Ar^{\bullet+}$ were compared with $(C_2,H_4,O_2)^{\bullet+}$ ions produced by electron transfer from acetic acid to $Ar^{\bullet+}$. The experimental results are shown in Figure 10.

Electron transfer from acetic acid to $CO^{\bullet+}$ (IE = 14.014 ± 0.0003) and $Ar^{\bullet+}$ (IE = 15.759 ± 0.001) was accompanied by considerable dissociation of the acetic acid cation (RE = 10.65 ± 0.02) into $CH_2CO^{\bullet+}$ + H_2O (and not CH_3CO^+ + OH). This observation is consistent with the preferential establishment of the more stable enol isomer, $CH_2C(OH)_2^{\bullet+}$, upon ionization of acetic acid as predicted by computations.[22] Small amounts of both the $CH_2CO^{\bullet+}$ and $CH_2C(OH)_2^{\bullet+}$ ions were observed to attach acetic acid at the flows of acetic acid that were employed.
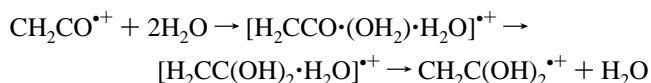
Figure 10 shows a good correlation in the onset energies for the loss of H_2O from the cation derived from acetic acid by electron transfer, $CH_2C(OH)_2^{\bullet+}$, and the loss of H_2O (HDO, D_2O) from the $(C_2,H_2,D_2,O_2)^{\bullet+}$ cation derived from the reaction of $CH_2CO^{\bullet+}$ with D_2O. The match in onset and product formation is reasonably convincing even though the CID measurements are somewhat crude. They involve multiple collisions with Ar atoms and some preliminary dehydration $(C_2,H_2,D_2,O_2)^{\bullet+}D_2O$ (see top left in Figure 10) and desolvation of $CH_2CO^{\bullet+}$(acetic acid) and $CH_2C(OH)_2^{\bullet+}$(acetic acid) (see bottom left and right in Figure 10). We can conclude from these similarities in the onsets and product formation that the product ions formed in the hydrolysis of ketene cations are those formed in the ionization of acetic acid.

6. Discussion and Conclusions

The spatial separation of spin and charge sites on a distonic radical cation allows a pronounced dual chemistry: the charge site may react as a cation whereas the spin site may react as a radical. Such dualism was previously shown by Tanko and Phillips for the reactions of radical anions and these authors suggested similar trends for radical cations.[27] In the case of the hydrolysis of ketene cations, the dual chemistry of the distonic radical cations can result in the formation of two different types of pre-reaction complexes. Hydration of ketene as a radical yields a π-complex complex, **2c**, which is unreactive toward hydrolysis whereas hydration of ketene as a cation yields ion–dipole complex, **2a**, which leads to the acetic acid cation.

The hydrolysis of the C=C or C=O bonds of $H_2CCO^{\bullet+}$ with a single water molecule via the pre-reaction ion–dipole complex, **2a**, yields keto, $H_3CCOOH^{\bullet+}$, or enolic, $H_2CC(OH)OH^{\bullet+}$, forms of ionized acetic acid, respectively. The reaction barriers are 32.7 and 17.8 kcal mol^{-1} above the dissociation limit to $H_2CCO^{\bullet+}$ + H_2O, respectively. The reaction barrier between canonic and enolic forms is 17.0 kcal mol^{-1} above the dissociation limit. Thus, the hydrolysis of ketene cations with a single water molecule cannot be observed under experimental conditions.

The attack of an additional water molecule on the [$CH_2CO\cdot H_2O$]$^{\bullet+}$ pre-reaction complex drops the barrier to the C–O hydrolysis dramatically. The water molecule acts as a catalyst to yield the hydrated enolic form of ionized acetic acid, [$H_2CC(OH)_2\cdot H_2O$]$^{\bullet+}$, via a proton-transport mechanism. This reaction is strongly exothermic (−51.0 kcal mol^{-1}); thus, a water molecule is released. Overall, the catalytic hydrolysis of the C–O bond of $H_2CCO^{\bullet+}$ proceeds efficiently with two water molecules:

$$CH_2CO^{\bullet+} + 2H_2O \rightarrow [H_2CCO\cdot(OH_2)\cdot H_2O]^{\bullet+} \rightarrow$$
$$[H_2CC(OH)_2\cdot H_2O]^{\bullet+} \rightarrow CH_2C(OH)_2^{\bullet+} + H_2O$$

Results of flow-reactor tandem mass spectrometer experiments in which $CH_2CO^{\bullet+}$ was produced either directly from ketene by electron transfer or by the chemical reaction of $CH_2^{\bullet+}$ with CO are consistent with formation of an $(C_2,H_4,O_2)^{\bullet+}$ ion

in a reaction second-order in H_2O. Furthermore, comparative multi-CID experiments indicate that this ion is likely to be the enolic $CH_2C(OH)_2^{\bullet+}$ which is derived by electron transfer from acetic acid.

The energetic barrier to 1,3 hydrogen shift between H_3-$CCOOH^{\bullet+}$ and $H_2CC(OH)OH^{\bullet+}$ decreases when H_2O is involved. Two possible mechanisms were examined: *proton-transport catalysis* where the water molecule acts as a carrier and "spectator" catalysis where a 1,3 hydrogen shift occurs in the presence of a water molecule as a mere spectator. The proton-transport mechanism is the most efficient and provides a sufficient decrease in the activation energy to drop the barrier below the dissociation limit to $H_3CCOOH^{\bullet+}$ and H_2O. Thus, the water molecule catalyzes the rearrangement from the higher-energy canonic to the lower-energy enolic form. However, for the reverse rearrangement, the activation barrier for the proton-transport mechanism is still above the dissociation limit to H_2-$CC(OH)_2^{\bullet+}$ and H_2O. Nevertheless, formation of neutral acetic acid should be possible by electron recombination with the water adduct, $[CH_2C(OH)_2 \cdot H_2O]^{\bullet+}$.

Formation of acetic acid cations from ketene cations and water by gas-phase chemistry second order in water will be unfavorable in the interstellar medium because of the low gas-phase density of water molecules. The encounter of the pre-reaction complex $[CH_2CO \cdot H_2O]^{\bullet+}$ with another gas-phase water molecule is therefore unlikely to occur before dissociation or recombination with electrons. However, gas-phase water molecules might not be the only possible catalyst for the formation of the acetic acid cation from the ketene cation. Indeed, recent FTIR experiments have demonstrated that water ice can act as a solid-phase catalyst in the H-atom transport catalysis for the isomerization of cyanamide into carbodiimide.[28] So water ice conceivably could catalyze the isomerization of the pre-reaction complex $[CH_2CO \cdot H_2O]^{\bullet+}$ into the acetic acid cation. Furthermore, the presence of ice also can promote electron−ion recombination to form acetic acid according to reaction 13. Icy surfaces would readily be available in hot cores and dense molecular clouds[29] in which neutral acetic acid has already been detected.[4]

$$CH_2C(OH)_2^{\bullet+} \text{ice} + e \rightarrow CH_3COOH + \text{ice} \qquad (13)$$

References and Notes

(1) Wincel, H.; Fokkens, R. H.; Nibbering, N. M. M. *Rapid Commun. Mass Spectrom.* **2000**, *14*, 135.

(2) Herbst, E. *Chem. Soc. Rev.* **2001**, *30*, 168.

(3) Blagojevic, V.; Petrie, S.; Bohme, D. K. *Mon. Not. R. Astron. Soc.* **2003**, *339*, L7.

(4) Mehringer, D. M.; Snyder, L. E.; Miao, Y. *ApJ* **1997**, *480*, L71.

(5) Nguyen, M. T.; Raspoet, G. *Can. J. Chem.* **1999**, *77*, 817.

(6) (a) Mackay, G. I.; Vlachos, G. D.; Bohme, D. K.; Schiff, H. I. *Int. J. Mass Spectrom. Ion Phys.* **1980**, *36,* 259. (b) Raksit, A. B.; Bohme, D. K. *Int. J. Mass Spectrom. Ion Processes* **1983/84**, *55*, 69. (c) Koyanagi, G. K.; Lavrov, V.; Baranov, V. I.; Bandura, D.; Tanner, S. D.; McLaren, J. W.; Bohme, D. K. *Int. J. Mass Spectrom.* **2000**, *194*, L1. (d) Koyanagi, G. K.; Baranov, V. I.; Tanner, Bohme, D. K. *J. Anal. At. Spectrom.* **2000**, *15*, 1207.

(7) Frisch, M. J.; Trucks, G. W.; Schlegel, H. B.; Scuseria, G. E.; Robb, M. A.; Cheeseman, J. R.; Zakrzewski, V. G.; Montgomery, J. A.; Stratmann, R. E.; Burant, J. C.; Dapprich, S.; Millam, J. M.; Daniels, A. D.; Kudin, K. N.; Strain, M. C.; Farkas, O.; Tomasi, J.; Barone, V.; Cossi, M.; Cammi, R.; Mennucci, B.; Pomelli, C.; Adamo, C.; Clifford, S.; Ochterski, J.; Petersson, G. A.; Ayala, P. Y.; Cui, Q.; Morokuma, K.; Salvador, P.; Dannenberg, J. J.; Malick, D. K.; Rabuck, A. D.; Raghavachari, K.; Foresman, J. B.; Cioslowski, J.; Ortiz, J. V.; Baboul, A. G.; Stefanov, B. B.; Liu, G.; Liashenko, A.; Piskorz, P.; Komaromi, I.; Gomperts, R.; Martin, R. L.; Fox, D. J.; Keith, T.; Al-Laham, M. A.; Peng, C. Y.; Nanayakkara, A.; Challacombe, M.; Gill, P. M. W.; Johnson, B. G.; Chen, W.; Wong, M. W.; Andres, J. L.; Gonzalez, C.; Head-Gordon, M.; Replogle, E. S.; Pople, J. A. *Gaussian98*, revision A.11; Gaussian, Inc.: Pittsburgh, PA, 2001.

(8) Becke, A. D. *J. Chem. Phys.* **1993**, *98*, 5648.

(9) Lee, C.; Yang, W.; Parr, R. G. *Phys., Rev. B* **1988**, *37*, 785.

(10) Hehre, W. J.; Ditchfield, R.; Pople, J. A. *J. Chem. Phys.* **1972**, *56*, 2257.

(11) Krishnan, R.; Binkley, J. S.; Seeger, R.; Pople, J. A. *J. Chem. Phys.* **1980**, *72*, 650.

(12) Chandrasekhar, J.; Andrade, J. G.; Schleyer, P. v. R. *J. Am. Chem. Soc.* **1981**, *103*, 5609.

(13) Clark, T.; Chandrasekhar, J.; Spitznagel, G. W.; Schleyer, P. v. R. *J. Comput. Chem.* **1983**, *4*, 294.

(14) Gonzalez, C.; Schlegel, H. B. *J. Chem. Phys.* **1989**, *90*, 3154.

(15) Gonzalez, C.; Schlegel, H. B. *J. Phys. Chem.* **1990**, *94*, 5523.

(16) Reed, A. E.; Weinstock, R. B.; Weinhold, F. *J. Chem. Phys.* **1985**, *83*, 735.

(17) Reed, A. E.; Weinhold, F. *J. Chem. Phys.* **1985**, *83*, 1736.

(18) Reed, A. E.; Curtiss, L. A.; Weinhold, F. *Chem. Rev.* **1988**, *88*, 899.

(19) Reed, A. E.; Schleyer, P. v. R. *J. Am. Chem. Soc.* **1990**, *112*, 1434.

(20) *GaussViewW*; Gaussian, Inc.: Pittsburgh, PA, 2001.

(21) Baranov, V. I.; Bohme, D. K. *Int J. Mass Spectrom. Ion Processes* **1996**, *154*, 71.

(22) (a) Bouma, W. J.; Nobes, R. H.; Radom, L. *J. Am. Chem. Soc.* **1982**, *104*, 2929. (b) Yates, B. F.; Bouma W. J.; Radom, L. *J. Am. Chem. Soc.* **1984**, *106*, 5805.

(23) Postma, R.; Ruttink, P. J. A.; Terlouw, J. K.; Holmes, J. L. *J. Chem. Soc. Chem. Commun.* **1986**, 683.

(24) (a) Mohr, M.; Zipse, H.; Marx, D.; Parinello, M. *J. Phys. Chem. A* **1997**, *101*, 8942. (b) Mohr, M.; Marx, D.; Parrinello, M.; Zipse, H. *Chem. Eur. J.* **2000**, *6*, 4009. (c) Mohr, M.; Zipse, H. *Phys. Chem. Chem. Phys.* **2001**, *3*, 1246.

(25) (a) Levesen, K.; Schwarz, H. *J. Chem. Soc., Perkins Trans.* 2 **1976**, 1231. (b) Holmes, J. L.; Lossing, F. P. *J. Am. Chem. Soc.* **1980**, *102*, 3732. (c) Heinrich, N.; Koch, W.; Frenking, G.; Schwarz, H. *J. Am. Chem. Soc.* **1986**, *108*, 593. (d) Caballol, Poblet, J. M.; Sarasa, J. P.; Olivella, S.; Sole, A. *J. Phys. Chem.* **1988**, *92*, 3336.

(26) Bohme, D. K. *Int. J. Mass. Spectrom. Ion Processes* **1992**, *115*, 95.

(27) Tanko, J. M.; Phillips, J. P. *J. Am. Chem. Soc.* **1999**, *121*, 6078.

(28) Duvernay, F.; Chiavassa, T.; Borget, F.; Aycard, J.-P. *J. Phys. Chem. A* **2005**, *109*, 603.

(29) Ehrenfreund, P.; Charnley, S. B. *Annu. Rev. Astron. Astrophys.* **2000**, *38*, 427.